Dalton Transactions

PAPER

View Article Online
View Journal | View Issue

Cite this: *Dalton Trans.*, 2014, **43**, 3842

Halogen effects on photoluminescence and catalytic properties: a series of spatially arranged trimetallic zinc(II) complexes†

Haeri Lee, Tae Hwan Noh and Ok-Sang Jung*

Received 6th November 2013,
Accepted 19th December 2013

DOI: 10.1039/c3dt53137f

www.rsc.org/dalton

Self-assembly of ZnX_2 (X = Cl, Br, and I) with *N*,*N*′,*N*″-tris(2-pyridinylethyl)-1,3,5-benzenetricarboxamide (L) as a tridentate N-donor ligand yields discrete C_3-symmetric trimetallic zinc(II) complexes, $[Zn_3X_6L(MeOH)_3]$. These form, *via* π···π interactions and NH···O=C hydrogen-bonds, an ensemble constituting a unique columnar stacking structure in an *abab*··· staggered fashion. For this series of complexes, the halogen effects on the photoluminescence, catalysis, and thermal properties were investigated. For $[Zn_3Cl_6L(MeOH)_3]$, a blue luminescence was observed at 462 nm (λ_{ex} = 369 nm). The transesterification catalysis showed significant halogen effects in the order $[Zn_3I_6L(MeOH)_3]$ > $[Zn_3Cl_6L(MeOH)_3]$ > $[Zn_3Br_6L(MeOH)_3]$ in methanol, whereas in a mixture of methanol and acetonitrile, the order was $[Zn_3I_6L(MeOH)_3]$ > $[Zn_3Br_6L(MeOH)_3]$ > $[Zn_3Cl_6L(MeOH)_3]$. Such notable different effects among the three complexes might be explained by the halogens' electronic effects and dissociation properties.

Introduction

Diverse polypyridyl N-donor ligands that can coordinate two or more remote metal centers have been used to construct desirable molecular structures.[1–4] Current applications of such polynuclear complexes span a wide range of interesting fields such as mixed-valence species, photo-induced electron or energy transfer, magnetic exchange between paramagnetic centers, and supramolecular weak interactions.[5–10] Specifically, tridentate N-donor building tectonics have been employed to synthesize cage coordination complexes or C_3-symmetric triangular module metal complexes.[11–18] Trimetallic complexes *via* tridentate ligand metal ions are relatively rare, unlike the vast majority of dinuclear complexes. Unique tridentate ligands containing pyridyl moieties, for example, offer, *via* the introduction of appropriate metal ions, wider opportunities for a trigonal metallic array. A number of such trimetallic complexes have been synthesized in recent years, especially those with a tridentate core.[19] Their hyper-branched structural and chemical features, with their advanced material and catalytic properties, have been a good prototype for generation of multifunctional properties.[20] Thus, systematic C_3-symmetric trimetallic complexes offer interesting physicochemical properties that have been found to be delicately dependent on the nature of the ligands and co-ligands.

In this context, in an investigation of the significant halogen effects of C_3-symmetric trimetallic complexes, ZnX_2 (X = Cl, Br, and I) was reacted with C_3-symmetric *N*,*N*′,*N*″-tris-(2-pyridinylethyl)-1,3,5-benzenetricarboxamide (L).[16] Further to this, a systematic series of trimetallic zinc(II) complexes and their one-dimensional (1D) ensemble crystal structures formed *via* intermolecular forces, along with the direct halogen effects on their photoluminescence, transesterification catalytic activity, and thermal properties, are reported herein. Zinc(II) complexes have been extensively examined for their use in appropriate tetrahedral binding Lewis acidity, metallo-enzymes, zinc finger proteins, transmetallation, and homogeneous catalysis.[21–28] A variety of zinc(II) coordination complexes containing aromatic moieties exhibit unique ligand-to-metal charge transfer luminescent properties that are strongly dependent on the geometry of the ligands and counteranions.[23,25] Furthermore, zinc(II) compounds with functional organic ligands can potentially be used in light-emitting-diode and heterogeneous-catalysis applications.[22]

Department of Chemistry, Pusan National University, Pusan 609-735, Korea. E-mail: oksjung@pusan.ac.kr; Fax: +82 51 516 7421; Tel: +82 51 510 2591

†Electronic supplementary information (ESI) available: The distances of weak inter- and intra-molecular interactions, ORTEP images, solid-state excitation spectra, photoluminescence spectra in Me_2SO of $[Zn_3Cl_6L(MeOH)_3]$, $[Zn_3Br_6L(MeOH)_3]$, and $[Zn_3I_6L(MeOH)_3]$; partial ^1H NMR spectra showing catalytic effects for transesterification of phenyl acetate using $[Zn_3I_6L(MeOH)_3]$; SEM images of calcined $[Zn_3I_6L(MeOH)_3]$ at 200 °C for 1 h, 400 °C for 1 h. CCDC 970293–970295. For ESI and crystallographic data in CIF or other electronic format see DOI: 10.1039/c3dt53137f

Experimental section

Materials and measurements

All chemicals including zinc(II) chloride, zinc(II) bromide, zinc(II) iodide, and phenyl acetate were purchased from Aldrich, and used without further purification. *N*,*N*′,*N*″-Tris-(2-pyridinylethyl)-1,3,5-benzenetricarboxamide (L) was prepared according to the method reported in the literature.[16] Elemental microanalyses (C, H, N) were performed on crystalline samples at the KBSI Pusan Center using a Vario-EL III. Thermal analyses were undertaken under a nitrogen atmosphere at a scan rate of 10 °C min^{-1} using a Labsys TGA-DSC 1600. The infrared spectra of samples prepared as KBr pellets were obtained on a Nicolet 380 FT-IR spectrophotometer. The ^{1}H NMR (300 MHz) spectra were recorded on a Varian Mercury Plus 300. Scanning electron microscopy (SEM) images were obtained on a Tescan VEGA 3. Powder X-ray diffraction data were recorded on a Rigaku RINT/DMAX-2500 diffractometer at 40 kV, 126 mA for Cu Kα. Excitation and emission spectra were acquired on a FluoroMate FS-2 spectrofluorometer. Fluorescence microscopy images were obtained with an Olympus BX51 microscope equipped with an AxioCam MRc 5 digital camera and a U-MWU2 filter set.

Preparation of $[Zn_3Cl_6L(MeOH)_3]$

A methanol solution (5 mL) of *N*,*N*′,*N*″-tris(2-pyridinylethyl)-1,3,5-benzenetricarboxamide (L) (78 mg, 0.15 mmol) was added to a methanol solution (5 mL) of zinc(II) chloride (61 mg, 0.45 mmol). Slow evaporation of the solvent produced colorless crystals of $[Zn_3Cl_6L(MeOH)_3]$ in a 76% (117 mg) yield after 3 days. mp 300 °C (dec.). Found: C, 38.3; H, 4.2; N, 8.1. Calc. for $C_{33}H_{42}Cl_6N_6O_6Zn_3$: C, 38.6; H, 4.2; N, 8.2%. IR (KBr pellet, cm^{-1}): 3585 (br), 3506 (br), 3367 (br), 3131 (br), 1635 (s), 1608 (s), 1548 (s), 1488 (s), 1440 (s), 1363 (m), 1307 (s), 1193 (w), 1160 (w), 1064 (w), 1024 (w), 779 (m).

Preparation of $[Zn_3Br_6L(MeOH)_3]$

This product was prepared in the same manner as $[Zn_3Cl_6L(MeOH)_3]$, using $ZnBr_2$ instead of $ZnCl_2$ in 73% (141 mg) yield. mp 303 °C (dec.). Found: C, 31.0; H, 3.2; N, 6.4. Calc. for $C_{33}H_{42}Br_6N_6O_6Zn_3$: C, 30.6; H, 3.3; N, 6.5%. IR (KBr pellet, cm^{-1}): 3500 (br), 3363 (br), 3077 (br), 1635 (s), 1608 (s), 1542 (s), 1488 (m), 1440 (m), 1307 (m), 1159 (w), 1064 (w), 1024 (w), 775 (m).

Preparation of $[Zn_3I_6L(MeOH)_3]$

The product also was prepared in the same manner as $[Zn_3Cl_6L(MeOH)_3]$, using ZnI_2 instead of $ZnCl_2$ in 72% (170 mg) yield. mp 303 °C (dec.). Found: C, 25.2; H, 2.6; N, 5.3. Calc. for $C_{33}H_{42}I_6N_6O_6Zn_3$: C, 25.1; H, 2.7; N, 5.3%. IR (KBr pellet, cm^{-1}): 3509 (br), 3378 (br), 3081 (br), 2798 (w), 1633 (s), 1608 (s), 1542 (s), 1486 (m), 1438 (m), 1307 (m), 1159 (w), 1064 (w), 1025 (w), 1002 (m), 759 (m).

Transesterification catalysis

Phenyl acetate (2.72 g, 2 mmol) was dissolved in methanol (15 mL) or a mixture of methanol and acetonitrile (15 mL, v/v = 1 : 1), and the catalysts (0.1 mmol; 34 mg for $[Zn_3Cl_6L(MeOH)_3]$; 43 mg for $[Zn_3Br_6L(MeOH)_3]$; 52 mg for $[Zn_3I_6L(MeOH)_3]$) were added to the reaction solution. The reaction solution was stirred at 50 °C for both 4 h and 6 h. The reaction using $[Zn_3I_6L(MeOH)_3]$ was achieved at reflux temperature. The conversion yields were monitored with reference to the ^{1}H NMR spectra. All of the reactions were run at least three times and the conversion yields are averaged.

Crystal structure determination

X-ray data were collected on a Bruker SMART automatic diffractometer equipped with graphite-monochromated Mo Kα radiation (λ = 0.71073 Å) and a CCD detector at −25 °C. Thirty-six frames of two-dimensional diffraction images were collected and processed to obtain the cell parameters and orientation matrix. The data were corrected for Lorentz and polarization effects. The absorption effects were corrected using the multi-scan method (SADABS).[29] The structures were solved using direct methods (SHELXS 97) and refined by full-matrix least squares techniques (SHELXL 97).[30] The non-hydrogen atoms were refined anisotropically, and the hydrogen atoms were placed in calculated positions and refined only for the isotropic thermal factors. The crystal parameters along with procedural information on the data collection and structure refinement are listed in Table 1.

Results and discussion

Synthesis

The reaction of ZnX_2 (X = Cl, Br, and I) with *N*,*N*′,*N*″-tris(2-pyridinylethyl)-1,3,5-benzenetricarboxamide (L) as a C_3-axis tridentate N-donor in methanol at room temperature afforded discrete C_3-symmetric trimetallic zinc(II) complexes, $[Zn_3X_6L(MeOH)_3]$, in high yields, as shown in Scheme 1. The reactions were initially conducted in the 1 : 1 mole ratio of zinc(II) : L, but the products were not significantly affected by either the mole ratio or concentrations, which indicated that they were thermodynamically stable species. These products are remarkable in that there was no evidence for coordination-polymerization, not even at high concentrations and despite the lack of protective groups. Thus, the discrete trimetallic complexes' formation might be attributable to the intrinsic properties of the reaction system. The crystalline products were not obtained in ethanol, *n*-propanol, or *i*-propanol instead of methanol. The colorless crystalline products of $[Zn_3X_6L(MeOH)_3]$ were air-stable and dissociated in methanol, ethanol, *N*,*N*-dimethylformamide, and dimethyl sulfoxide, but insoluble in water, *n*-hexane, dichloromethane, chloroform, and acetone. The results of an elemental analysis and the products' NMR spectra were consistent with desirable structures.

Table 1 Crystallographic data and structure refinement for $[Zn_3Cl_6L(MeOH)_3]$, $[Zn_3Br_6L(MeOH)_3]$, and $[Zn_3I_6L(MeOH)_3]$

	$[Zn_3Cl_6L(MeOH)_3]$	$[Zn_3Br_6L(MeOH)_3]$	$[Zn_3I_6L(MeOH)_3]$
Formula	$C_{33}H_{42}Cl_6N_6O_6Zn_3$	$C_{33}H_{42}Br_6N_6O_6Zn_3$	$C_{33}H_{42}I_6N_6O_6Zn_3$
M_w	1027.54	1294.30	1576.24
Crystal system	Hexagonal	Hexagonal	Hexagonal
Space group	$P6_3$	$P6_3$	$P6_3$
a/Å	32.1306(4)	31.5420(3)	31.9496(2)
c/Å	7.3880(1)	7.6862(1)	8.0211(1)
V/Å^3	6605.3(2)	6622.5(1)	7090.8(1)
Z	6	6	6
ρ/g cm^{-3}	1.550	1.947	2.215
μ/mm^{-1}	2.032	7.094	5.473
$F(000)$	3132	3780	4428
R_{int}	0.0824	0.0629	0.0427
GoF on F^2	1.064	1.115	1.188
R_1 $[I > 2\sigma(I)]^a$	0.0448	0.0419	0.0529
wR_2 (all data)^b	0.1045	0.0890	0.0923

$^a R_1 = \sum||F_o| - |F_c||/\sum|F_o|$. ^{b} w$R_2 = (\sum[w(F_o^2 - F_c^2)^2]/\sum[w(F_o^2)^2])^{1/2}$.

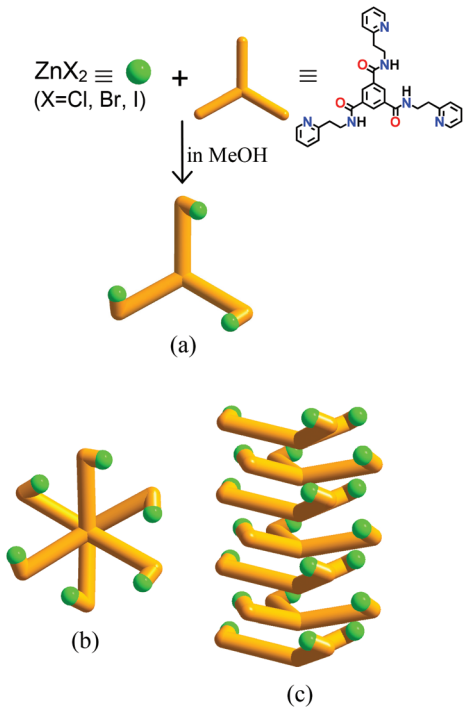

Scheme 1 Synthetic scheme of trimetallic zinc(II) complexes (a). Top view (b) and side view (c) of columnar stacking structure.

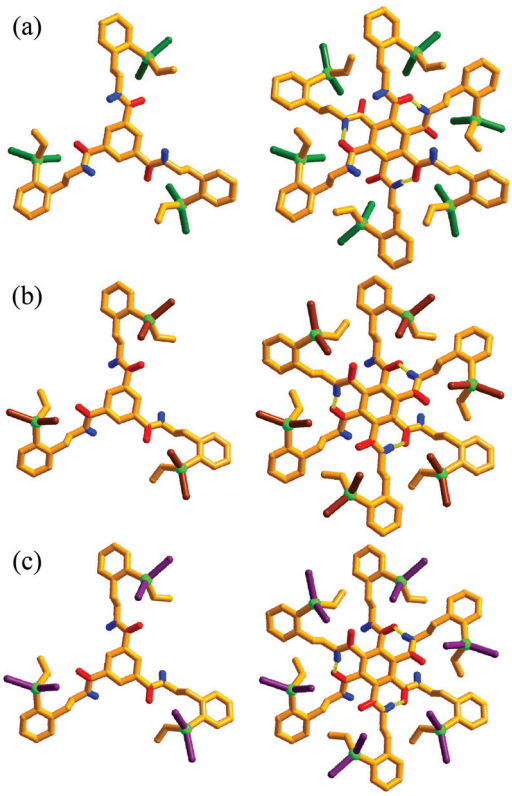

Fig. 1 Top views of single (left) and double (right) molecules of $[Zn_3Cl_6L(MeOH)_3]$ (a), $[Zn_3Br_6L(MeOH)_3]$ (b), and $[Zn_3I_6L(MeOH)_3]$ (c).

Crystal structures

The crystal structures of $[Zn_3X_6L(MeOH)_3]$ are basically isostructural hexagonal $P6_3$ space groups, as depicted in Fig. 1 and S1 (see ESI†), and the relevant bond lengths and angles are listed in Table 2. Their bond lengths and angles around the zinc(II) ion differ slightly, presumably owing to the different electronic and steric effects of the halides. The local geometry around the zinc(II) ion approximates to a typical tetrahedral arrangement with two halides (X–Zn–X = 116.29(5)–127.00(5)°), a nitrogen from L, and an oxygen from the methanol molecule. The L connects three zinc(II) ions to form C_3-axis trimetallic $[Zn_3X_6L(MeOH)_3]$. The methanol molecule acts as the fourth ligand rather than a simple solvate molecule. The intramolecular Zn···Zn distances of $[Zn_3Cl_6L(MeOH)_3]$, $[Zn_3Br_6L(MeOH)_3]$, and $[Zn_3I_6L(MeOH)_3]$ are 11.981(3)–12.0573(8) Å, 12.304(1)–12.521(1) Å, and 12.509(2)–12.675(2) Å, respectively. Intramolecular interactions of MeOH···O=C (1.78–1.79 Å for $[Zn_3Cl_6L(MeOH)_3]$; 1.81–1.85 Å for $[Zn_3Br_6L(MeOH)_3]$; 1.74–1.91 Å for $[Zn_3I_6L(MeOH)_3]$) exist in the solid state (Fig. 1). All of the products showed an infinite 1D column ensemble *via* close intermolecular π···π contacts (3.6839(5)–

Table 2 Selected bond distances (Å) and bond angles (°) for $[Zn_3Cl_6L(MeOH)_3]$, $[Zn_3Br_6L(MeOH)_3]$, and $[Zn_3I_6L(MeOH)_3]$

	$[Zn_3Cl_6L(MeOH)_3]$	$[Zn_3Br_6L(MeOH)_3]$	$[Zn_3I_6L(MeOH)_3]$
Zn(1)–N(1)	2.061(3)	2.043(5)	2.044(7)
Zn(1)–O(2)	1.988(3)	2.050(5)	2.052(6)
Zn(1)–X(1)	2.199(1)	2.338(1)	2.569(1)
Zn(1)–X(2)	2.229(1)	2.368(1)	2.529(1)
Zn(2)–N(3)	2.121(4)	2.040(4)	2.058(7)
Zn(2)–O(4)	2.018(4)	2.044(5)	2.032(7)
Zn(2)–X(3)	2.225(2)	2.3419(8)	2.577(1)
Zn(2)–X(4)	2.179(2)	2.3729(9)	2.523(1)
Zn(3)–N(5)	2.053(3)	2.036(4)	2.042(7)
Zn(3)–O(6)	2.015(3)	2.053(5)	2.026(6)
Zn(3)–X(5)	2.194(1)	2.3398(8)	2.536(1)
Zn(3)–X(6)	2.225(1)	2.3769(9)	2.578(1)
N(1)–Zn(1)–O(2)	110.2(1)	112.8(2)	103.1(3)
N(1)–Zn(1)–X(1)	110.1(1)	107.0(2)	112.8(2)
N(1)–Zn(1)–X(2)	109.0(1)	108.5(2)	112.5(2)
X(1)–Zn(1)–X(2)	118.7(5)	127.00(5)	116.29(5)
N(3)–Zn(2)–O(4)	107.8(2)	106.2(2)	111.2(3)
N(3)–Zn(2)–X(3)	110.7(1)	110.32(1)	104.9(2)
N(3)–Zn(2)–X(4)	109.0(1)	112.5(1)	111.5(2)
X(3)–Zn(2)–X(4)	120.1(9)	118.80(4)	124.38(5)
N(5)–Zn(3)–O(6)	107.8(1)	102.5(2)	100.2(3)
N(5)–Zn(3)–X(5)	108.93(9)	111.9(1)	112.9(2)
N(5)–Zn(3)–X(6)	110.61(9)	112.8(1)	114.6(2)
X(5)–Zn(3)–X(6)	120.84(5)	118.59(4)	116.90(5)

3.7041(5) Å for $[Zn_3Cl_6L(MeOH)_3]$; 3.83(4)–3.86(4) Å for $[Zn_3Br_6L(MeOH)_3]$; 3.954(4)–4.011(4) Å for $[Zn_3I_6L(MeOH)_3]$) and intermolecular hydrogen-bondings (2.21–2.25 Å or $[Zn_3Cl_6L(MeOH)_3]$; 2.30–2.39 Å for $[Zn_3Br_6L(MeOH)_3]$; 2.36–2.69 Å for $[Zn_3I_6L(MeOH)_3]$) between NH···O=C in an *abab*··· layer (Fig. 2). The π···π interactions and hydrogen-bondings were comparable to the results reported by Valencia *et al.*[31] and Jung *et al.*,[15] respectively. The columns were arranged in a hexagonal packing mode, as depicted in Fig. 3. Thus, the slightly different bond lengths and angles showed significant halogen effects. No other exceptional features, neither with respect to bond lengths nor to angles, were observed. The three tetrahedral zinc(II) moieties are in a propeller-like arrangement in the same upside direction from the central benzene. Accordingly, $[Zn_3Br_6L(MeOH)_3]$ and $[Zn_3I_6L(MeOH)_3]$ are chiral crystalline solids consisting of two-column *P*-helices and one-column *M*-helices (where *P* denotes right-handed helices and *M* denotes left-handed helices), whereas $[Zn_3Cl_6L(MeOH)_3]$ is a crystalline solid consisting of one-column *P*-helices and two-column *M*-helices. All of the crystals in the reaction vessel were a mixture of chiral crystals and enantiomeric crystals.

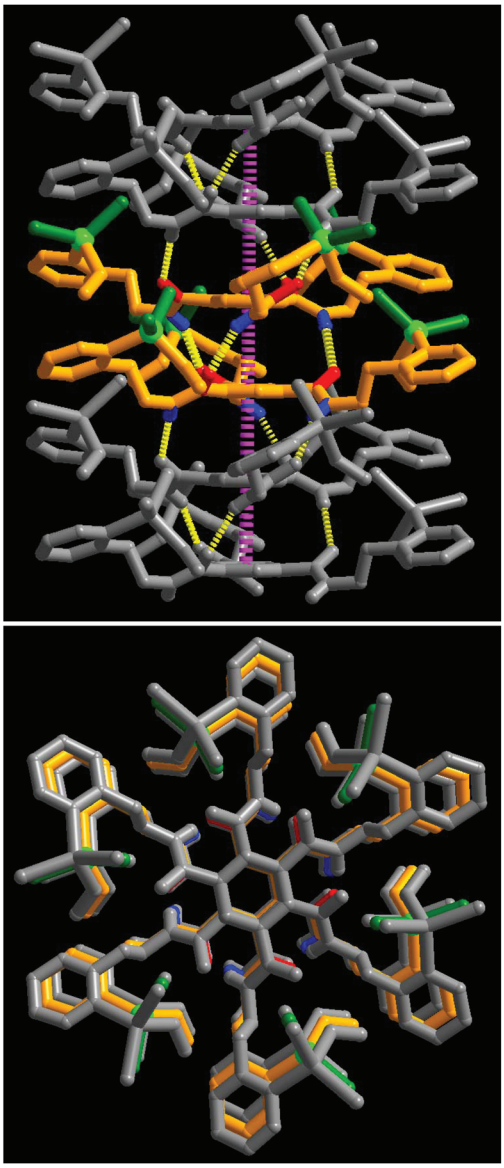

Fig. 2 Side view (top) and top view (bottom) of columnar $[Zn_3Cl_6L(MeOH)_3]$. The pink and yellow dashed lines denote the intermolecular π···π interactions and NH···O=C hydrogen-bonds, respectively.

Construction principle

By the reaction of ZnX_2 with L in methanol, discrete C_3-symmetric trimetallic zinc(II) complexes, $[Zn_3X_6L(MeOH)_3]$, not coordination polymeric species, were obtained in high yields. The present complexes were favorably formed irrespective of concentrations or mole ratios, indicating the thermodynamic stability of their skeletal structures. However, as noted already in the "Synthesis" section above, a solvent is an important factor in the formation of trimetallic complex crystals. What is the critical driving force behind the formation of the discrete trimetallic complexes rather than coordination polymers? A combination of tetrahedral zinc(II) ions and the appropriate tridentate N-donors seems to be a crucial factor. Specifically, formation might be attributable to the *ortho*-pyridyl N-donor of L. That is, such an N-donor might be an obstacle to the formation of coordination polymers. Moreover, intramolecular hydrogen-bonding between MeOH···O=C perhaps partially contributes to the formation of discrete trimetallic species. This would explain the key role of methanol in the self-assembly system. Another important feature is that both the intermolecular NH···O=C hydrogen-bonds and the π···π interactions can be attributed to the formation of the thermodynamically

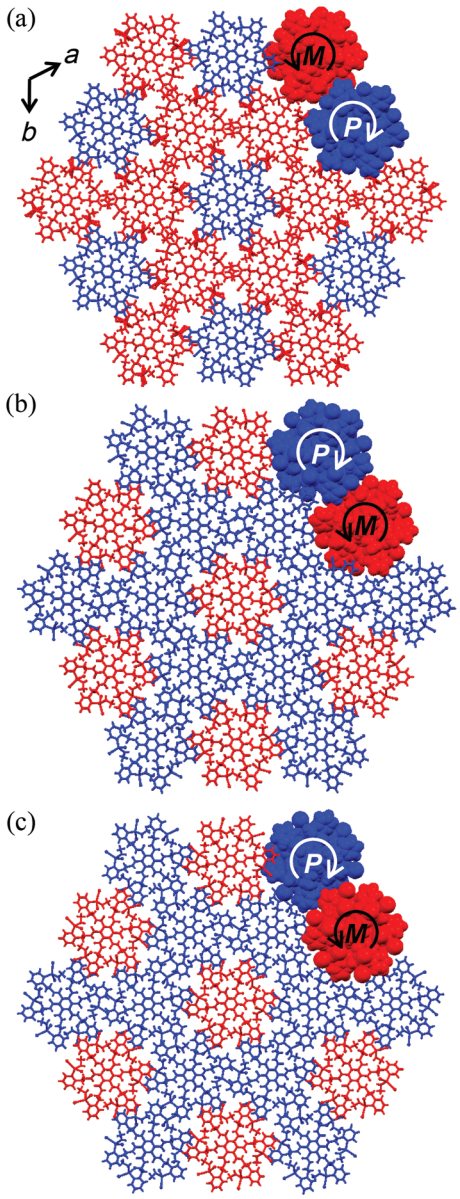

Fig. 3 Packing diagrams of $[Zn_3Cl_6L(MeOH)_3]$ (a), $[Zn_3Br_6L(MeOH)_3]$ (b), and $[Zn_3I_6L(MeOH)_3]$ (c). Red: *M*-helical column; blue: *P*-helical column.

stable columnar *abab*··· staggered stacking ensemble. As the present system did not reveal significant angle strains, we considered the formation of the overall crystalline structure to be due in part to the felicitous "weak interactions" rather than to the characteristics of the "geometry around the zinc(II) ion".

Photoluminescence

Great attention recently has been paid to d^{10} metal complexes, given their variety of applications in chemical sensors, photochemistry, and electroluminescent display.[32] The excitation and emission spectra of the present zinc(II) complexes then, together with those of L, were measured in the solid state at room temperature (Fig. 4 and S2, see ESI†). Emissions were observed at 462 nm (λ_{ex} = 421 nm) for $[Zn_3Cl_6L(MeOH)_3]$, 466 nm (λ_{ex} = 401 nm) for $[Zn_3Br_6L(MeOH)_3]$, and 482 nm (λ_{ex} = 372 nm) for $[Zn_3I_6L(MeOH)_3]$. The emission bands of $[Zn_3Cl_6L(MeOH)_3]$ and $[Zn_3Br_6L(MeOH)_3]$ were blue-shifted relative to the corresponding ligand L (λ_{em} = 480 nm; λ_{ex} = 421 nm), while $[Zn_3I_6L(MeOH)_3]$ was red-shifted. The ligand's intrinsic characteristics play a pivotal role in the photoluminescence mechanism of the present zinc(II) complexes. These results suggest that the complexes' emission bands can be ascribed to the ligand-to-metal charge transfer (LMCT).[33,34] The red-shift from $[Zn_3Cl_6L(MeOH)_3]$ to $[Zn_3I_6L(MeOH)_3]$ can be explained by the electronic effects of halides and the coordination environments of the zinc(II) ions.[35–37] And it is worthwhile, additionally, to mention that $[Zn_3Cl_6L(MeOH)_3]$ showed much stronger emissions than those of $[Zn_3Br_6L(MeOH)_3]$ and $[Zn_3I_6L(MeOH)_3]$ at room temperature. Such a significant difference can be attributed to the effective increase of the Zn–Cl bond rigidity and the reduction in the loss of energy through radiation-less decay. However, the quantum yield of $[Zn_3Cl_6L(MeOH)_3]$ (0.084%) is lower than that of the known iridium(III) complex, FIrpic (0.42%).[38] In order to achieve, *via* the inter-molecular NH···O=C hydrogen-bonds and the π···π interaction, the ensemble effect on the photoluminescence, their solution spectra were measured in Me_2SO, resulting in partial dissociation (see ESI†).

Transesterification catalysis

In order to investigate the halogen effects on the catalytic reactions, the $[Zn_3X_6L(MeOH)_3]$ series have been employed as a homogeneous catalyst of the transesterification reaction of phenyl acetate with methanol. Various catalysts available for transesterification of a wide range of esters with alcohol under mild conditions have been developed.[27,28] In the present investigation, $[Zn_3X_6L(MeOH)_3]$ (X = Cl, Br, and I) (0.1 mmol) significantly catalyzed the transesterification of phenyl acetate

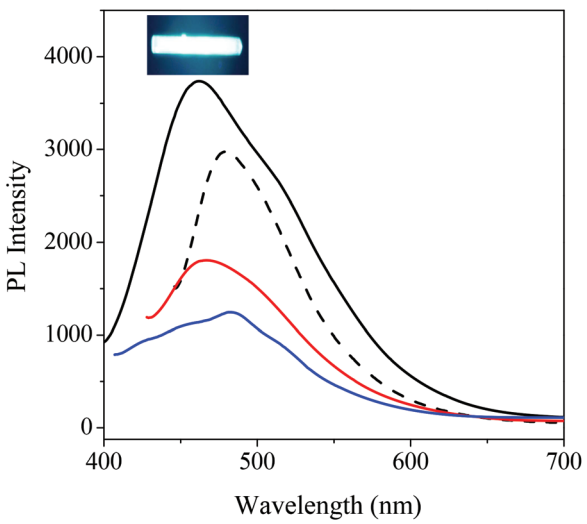

Fig. 4 Solid-state photoluminescence spectra of L (dashed line), $[Zn_3Cl_6L(MeOH)_3]$ (black solid line), $[Zn_3Br_6L(MeOH)_3]$ (red solid line), and $[Zn_3I_6L(MeOH)_3]$ (blue solid line) at room temperature. Inset: fluorescent-microscopic image of $[Zn_3Cl_6L(MeOH)_3]$.

(2 mmol) with an excess amount of methanol at 50 °C for 4 h or 6 h, as depicted in Fig. 5. A control reaction without the catalysts, meanwhile, showed trace amounts of ester-converted product. Another catalytic reaction with authentic ZnI_2 exhibited 13.8% conversion yield at 50 °C for 6 h. The catalysis process was monitored with reference to the ^{1}H NMR spectra (see ESI†). The trimetallic zinc(II) complexes showed, on catalytic activity in methanol, significant halogen effects in the order $[Zn_3I_6L(MeOH)_3]$ > $[Zn_3Cl_6L(MeOH)_3]$ > $[Zn_3Br_6L(MeOH)_3]$. The coordinated (activated) methanol molecule might be a key factor in transesterification. Of course, the 6 h catalysis showed a higher conversion than that of 4 h. It seems that the catalytic effects, as plotted for the present case in Fig. 5, are strongly dependent on the dissociation of the Zn–X bonds. It is not easy to elucidate the exact mechanism of catalysis at this stage, though the mechanism of metal-ion-catalyzed transesterification probably involves electrophilic activation of the carbon center of the carbonyl moiety by binding of the metal to the carbonyl oxygen.[28] If so, the vacant site and the Lewis acidity of the zinc metal center, accordingly, play important roles in this catalytic reaction. Thus, the process of leaving group's dissociation seems to be one of the conversion-rate-determining steps. And if this is the case, the catalysis reaction will show significant solvent effects. Therefore, in the present study, the catalysis reaction was carried out in a mixture of methanol and acetonitrile instead of (only) methanol; the resulting activity order was $[Zn_3I_6L(MeOH)_3]$ > $[Zn_3Br_6L(MeOH)_3]$ > $[Zn_3Cl_6L(MeOH)_3]$. That is, $[Zn_3I_6L(MeOH)_3]$ and $[Zn_3Br_6L(MeOH)_3]$ showed high activity in the mixture solvent whereas $[Zn_3Cl_6L(MeOH)_3]$ demonstrated high activity in the methanol. This result suggests that Zn–Cl is less dissociated in the mixture solvent than in methanol whereas Zn–I and Zn–Br are more dissociated in the mixture solvent than in methanol. The catalysis showed significant halogen effects both for the activity with respect to the solvent. With $[Zn_3I_6L(MeOH)_3]$, the 4 h reflux-temperature catalytic reaction in the mixture solvent effected complete conversion.

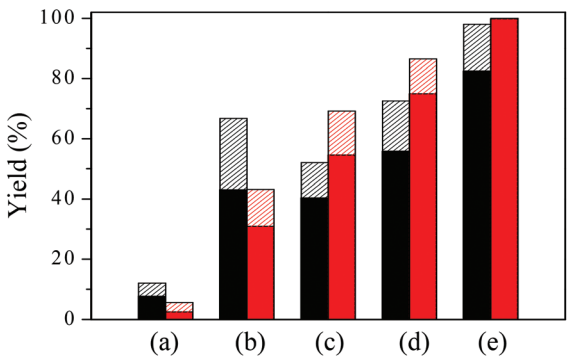

Fig. 5 Transesterification of phenyl acetate by methanol without catalyst (a), in the presence of $[Zn_3Cl_6L(MeOH)_3]$ (b), $[Zn_3Br_6L(MeOH)_3]$ (c), and $[Zn_3I_6L(MeOH)_3]$ (d) all at 50 °C, and in the presence of $[Zn_3I_6L(MeOH)_3]$ at reflux temperature (e). Black column: catalysis in methanol; red column: mixture of methanol and acetonitrile (v/v = 1 : 1); filled: catalysis for 4 h; dashed: catalysis for 6 h.

Thermal properties

The thermogravimetric analysis results for $[Zn_3X_6L(MeOH)_3]$ are plotted in Fig. 6. As can be seen, the skeletal structure was stable up to 300 °C before collapsing within the 300–550 °C range. The high collapse temperature can be attributed to the angle-strain-free structure. The coordinated methanol molecules began to evaporate at 104 °C (weight loss found: 9.2%; calcd: 9.4%) for $[Zn_3Cl_6L(MeOH)_3]$, at 162 °C (found: 8.8%; calcd: 7.4%) for $[Zn_3Br_6L(MeOH)_3]$, and at 171 °C (found: 6.2%; calcd: 6.1%) for $[Zn_3I_6L(MeOH)_3]$. This triggered

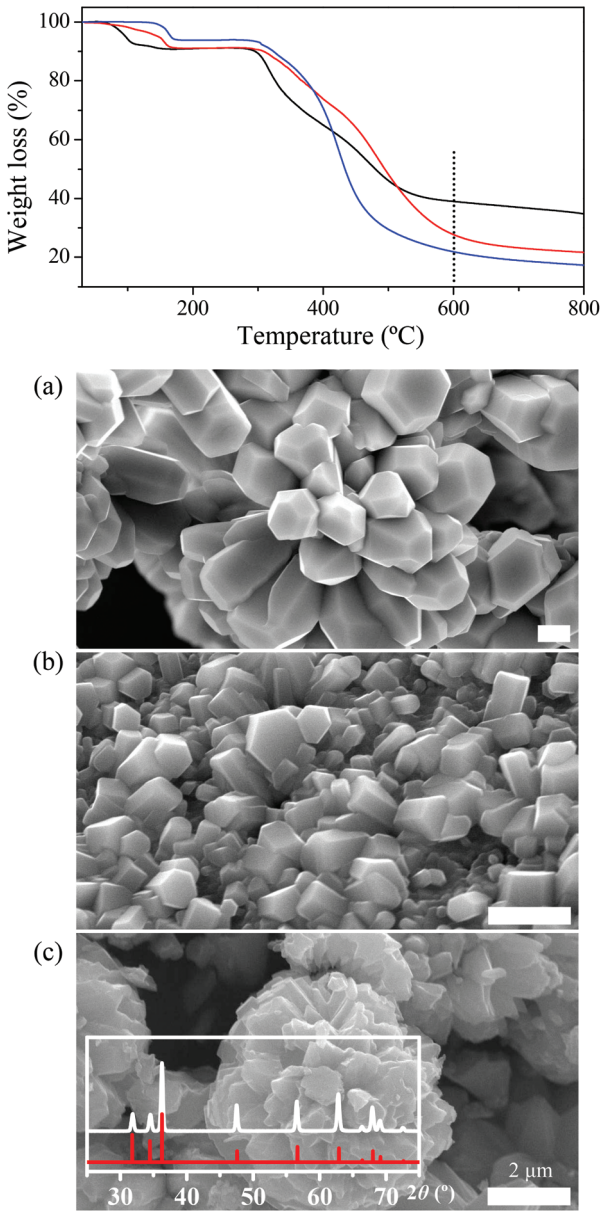

Fig. 6 Top: TGA curves of $[Zn_3Cl_6L(MeOH)_3]$ (black), $[Zn_3Br_6L(MeOH)_3]$ (red), and $[Zn_3I_6L(MeOH)_3]$ (blue); bottom: morphologies of the residues of $[Zn_3Cl_6L(MeOH)_3]$ (a), $[Zn_3Br_6L(MeOH)_3]$ (b), and $[Zn_3I_6L(MeOH)_3]$ (c) after calcination at 600 °C for 4 h. Inset: powder XRD data for zinc(II) oxide residue (white) and reference pattern (red) from ICDD database (PDF no. 36-1451).

significant halogen effects. In order to confirm the morphology change of the crystals during the skeletal collapse, all of the crystalline samples were monitored by SEM. It was found that all of the crystals ultimately had changed to zinc(II) oxide crystals, but that their morphologies differed according to the halogens. Images of the zinc(II) oxide crystals are provided in Fig. 6. Calcination for 1, 1, and 4 h at 200, 400, and 600 °C, respectively, effected contraction *via* eruption of both coordinated and burned organic molecules, thus producing the characteristic morphologies (see ESI†). The SEM images revealed that for $[Zn_3I_6L(MeOH)_3]$, the complex melted after the 200 °C calcination, and that at 400 °C, the compound changed to zinc (II) oxide micro-crystals of 1–5 μm size, which fact was confirmed by SEM-EDS; finally, at 600 °C, differently shaped zinc(II) oxide submicro-crystals formed. These results established that this method is an efficient means of morphological control of zinc(II) oxide crystals *via* structural difference. According to the SEM-EDS and powder X-ray diffraction pattern results, the final crystalline solids consisted of zinc(II) oxide. Zinc(II) oxide is widely used as an additive in numerous materials and products including plastics, ceramics, glass, cement, lubricants, paints, ointments, adhesives, sealants, pigments, foods (zinc-nutrient sources), batteries, ferrites, fire retardants, and first aid bandages. In materials science, different morphologies of zinc(II) oxide crystals serve task-specific functions such as in wide-band gap semiconductors of good transparency, high electron mobility, and strong room-temperature luminescence.[39]

Conclusions

Reaction of zinc(II) halides with a C_3-symmetric tridentate N-donor ligand afforded C_3-symmetric trimetallic zinc(II) complexes. This system appears to represent an important conceptual advance in the development of new discrete symmetric trimetallic complexes, not coordination polymers, *via* unique inter- and intra-molecular interactions.

Their photoluminescence properties show significant halogen effects, and $[Zn_3Cl_6L(MeOH)_3]$ particularly shows a blue emission. These compounds are potential candidates for incorporation into luminescent sensors and photoactive materials (*e.g.*, for detection of aromatic organic molecules). This catalysis work reveals that both direct halogen effects and solvent systems play very important roles in transesterification. Calcination of the materials results in formation of different morphologies of zinc(II) oxide. More systematic studies, for example on the synthesis of related ligands, are in progress. Further experiments, moreover, will provide more detailed information on the enormous potentials of the complexes' catalytic properties and photoluminescence.

Acknowledgements

This work was supported by a National Research Foundation of Korea (NRF) grant funded by the Korean Government [MEST] (2013-067841).

Notes and references

1 E. C. Constable, *Tetrahedron*, 1992, **48**, 10013–10059.
2 N. B. Debata, D. Tripathy and D. K. Chand, *Coord. Chem. Rev.*, 2012, **256**, 1831–1945.
3 R. Chakrabarty, P. S. Mukherjee and P. J. Stang, *Chem. Rev.*, 2011, **111**, 6810–6918.
4 W. L. Leong and J. J. Vittal, *Chem. Rev.*, 2011, **111**, 688–764.
5 C. Janiak, *Dalton Trans.*, 2003, 2781–2804.
6 N. G. R. Hearns, J. L. Koecok, M. M. Paquette and K. E. Preuss, *Inorg. Chem.*, 2006, **45**, 8817–8819.
7 M. Grazel, *Inorg. Chem.*, 2005, **44**, 6841–6851.
8 V. J. Catalano, W. E. Larson, M. M. Olmstead and H. B. Gray, *Inorg. Chem.*, 1994, **33**, 4502–4509.
9 A. I. Baba, H. E. Ensley and R. H. Schmehl, *Inorg. Chem.*, 1995, **34**, 1198–1207.
10 A. J. Amoroso, A. M. W. C. Thomson, J. P. Maher, J. A. McCleverty and M. D. Ward, *Inorg. Chem.*, 1995, **34**, 4828–4835.
11 T. H. Noh, E. Heo, K. H. Park and O.-S. Jung, *J. Am. Chem. Soc.*, 2011, **133**, 1236–1239.
12 M. Fujita, N. Fujita, K. Ogura and K. Yamagichi, *Nature*, 1999, **400**, 52–55.
13 S. Ghosh and P. S. Mukherjee, *J. Org. Chem.*, 2006, **71**, 8412–8416.
14 D. Moon, S. Kang, J. Park, K. Lee, R. P. John, H. Won, G. H. Seong, Y. S. Kim, H. Rhee and M. S. Lah, *J. Am. Chem. Soc.*, 2006, **128**, 3530–3531.
15 H. Lee, T. H. Noh and O.-S. Jung, *Angew. Chem., Int. Ed.*, 2013, **52**, 11790–11795.
16 H. Lee, T. H. Noh and O.-S. Jung, *CrystEngComm*, 2013, **15**, 1832–1835.
17 W. Hong, H. Lee, T. H. Noh and O.-S. Jung, *Dalton Trans.*, 2013, **42**, 11092–11099.
18 S. Hasegawa, S. Horike, R. Matsuda, S. Furukawa, K. Mochizuki, Y. Kinoshita and S. Kitagawa, *J. Am. Chem. Soc.*, 2007, **129**, 2607–2614.
19 H. Xia, T. B. Wen, Q. Y. Hu, X. Wang, X. Chen, L. Y. Shek, I. D. Williams, K. S. Wong and G. Jia, *Organometallics*, 2005, **24**, 562–569.
20 N. J. Long and C. K. Williams, *Angew. Chem., Int. Ed.*, 2003, **42**, 2586–2617.
21 A. W. Kleij, M. Kuil, D. M. Tooke, M. Lutz, A. L. Spek and J. N. H. Reek, *Chem.–Eur. J.*, 2005, **11**, 4743–4750.
22 J. W. Shin, J. M. Bae, C. Kim and K. S. Min, *Inorg. Chem.*, 2013, **52**, 2265–2267.
23 S. P. Jang, J. I. Poong, S. H. Kim, T. G. Lee, J. Y. Noh and C. Kim, *Polyhedron*, 2012, **33**, 194–202.
24 S. Enthaler, *ACS Catal.*, 2013, **3**, 150–158.
25 T. M. McCormick and S. Wang, *Inorg. Chem.*, 2008, **47**, 10017–10024.
26 W. N. Lipscomb and N. Strater, *Chem. Rev.*, 1996, **96**, 2375–2434.
27 C. A. Grapperhaus, T. Tuntulani, J. H. Reibenspies and M. Y. Darensbourg, *Inorg. Chem.*, 1998, **37**, 4052–4058.

28 L. S. Felices, E. C. Escudero-Adan, J. Benet-Buchholz and A. W. Kleij, *Inorg. Chem.*, 2009, **48**, 846–853.
29 G. M. Sheldrick, *SADABS, A Program for Empirical Absorption Correction of Area Detector Data*, University of Göttingen, Germany, 1996.
30 G. M. Sheldrick, *SHELXS-97: A Program for Structure Determination*, University of Göttingen, Germany, 1997; G. M. Sheldrick, *SHELXL-97: A Program for Structure Refinement*, University of Göttingen, Germany, 1997.
31 L. Valencia, P. Pérez-Lourido, R. Bastida and A. Macías, *Cryst. Growth Des.*, 2008, **8**, 2080–2082.
32 P. Jiang and Z. Guo, *Coord. Chem. Rev.*, 2004, **248**, 205–229.
33 B. Valeur, in *Molecular Fluorescence: Principles and Applications*, Wiley-VCH, Weinheim, 2002.
34 S. L. Zheng, M. L. Tong and X. M. Chen, *J. Chem. Soc., Dalton Trans.*, 2001, 586–592.
35 J. Luo, W. S. Li, P. Xu, L. Y. Zhang and Z. N. Chen, *Inorg. Chem.*, 2012, **51**, 9508–9516.
36 H. Kunkely and A. Vogler, *Chem. Phys. Lett.*, 2003, **376**, 226–229.
37 A. Horváth, C. E. Wood and K. L. Stevenson, *J. Phys. Chem.*, 1994, **98**, 6490–6495.
38 C. Adachi, R. C. Kwong, P. Djurovich, V. Adamovich, M. A. Baldo, M. E. Thompson and S. R. Forrest, *Appl. Phys. Lett.*, 2001, **79**, 2082–2084.
39 A. Hernandezbattez, R. Gonzalez, J. Viesca, J. Fernandez, J. Diazfernandez, A. MacHado, R. Chou and J. Riba, *Wear*, 2008, **265**, 422–428.